NMR Relaxation Study of the Complex Formed Between CBP and the Activation Domain of the Nuclear Hormone Receptor Coactivator ACTR†

Marc-Olivier Ebert,‡ Sung-Hun Bae, H. Jane Dyson, and Peter E. Wright*

Department of Molecular Biology and The Skaggs Institute for Chemical Biology, The Scripps Research Institute, 10550 North Torrey Pines Road, La Jolla, California 92037

Received August 29, 2007; Revised Manuscript Received November 21, 2007

ABSTRACT: Overexpression of the p160 steroid receptor coactivator ACTR is associated with breast and ovarian cancers. Complex formation between ACTR and the general transcriptional coactivators CBP and p300 plays a key role in the nuclear receptor-dependent regulation of gene transcription and was the first reported example of mutual synergistic folding of two disordered polypeptide chains. In order to investigate the structure and dynamics of the free domains and complex, we measured and analyzed ^{15}N longitudinal and transverse relaxation rates and [^{1}H]−^{15}N heteronuclear Overhauser effects of the backbone amides of the free and bound forms of human ACTR (residues 1041−1088) and mouse CBP (residues 2059−2117). Secondary chemical shifts for the free and bound forms were well correlated with the extent of backbone flexibility. The free ACTR domain has no residual secondary structure and shows all of the characteristics of a completely unfolded polypeptide chain. The free CBP domain retains most of the α-helical content seen in the complex but is significantly more flexible. Despite the disordered nature of the free individual domains, the complex has the motional characteristics of a completely folded protein complex and has no significant residual backbone fluctuation that might compensate for the massive loss of conformational entropy upon complex formation.

Hormone-regulated activation of gene transcription is a complex process that starts with binding of the ligand-activated receptor to the hormone response element in the promoter region of the gene, involves interaction with different coactivator complexes, and finally results in the recruitment of the basal transcription machinery (*1*−*4*). The p160 steroid receptor coactivator complex (SRC[1]) plays an important role in this process by catalyzing the histone acetylation and methylation that is required for remodeling of chromatin structure. This complex includes the general transcription activator CBP/p300 and one of three different SRCs called NcoA-1 (SRC-1), GRIP1/TIF2/NcoA-2 (SRC-2), and ACTR/AIB1/pCIP/RAC3/TRAM1 (SRC-3) which interact directly with the hormone receptor through three conserved LXXLL motifs (*5*−*7*). ACTR/AIB1 was initially discovered as a protein that is overexpressed in a high percentage of breast and ovarian cancers (*8*). Mice with a null mutation for the mouse homologue of ACTR showed abnormal development and function of the female reproductive system and reduced adult body size (*9*). Recent results showed that ACTR/AIB1 is an oncogene and that its overexpression leads to mammary carcinomas in transgenic mice (*10*). ACTR is also involved in proliferation of cancer (*11*, *12*), and a high level of ACTR is associated with tamoxifen resistance in patients (*13*). ACTR plays an important role in the development and progression of breast cancer and inhibition of ACTR function could result in an effective treatment of mammary carcinomas (*10*).

The structure of the complex between the coactivator binding domain of CBP and the transcriptional activation domain (AD) 1 of ACTR was determined by NMR (*14*) (Figure 1). In the free state, both domains are intrinsically disordered but fold upon formation of the complex (*14*, *15*). This complex provided the first example of mutual synergistic folding of two incompletely structured protein domains. With a dissociation constant (K_d) of 34 nM and $T\Delta S$ of −21.3 kcal/mol, its formation is purely enthalpy driven. Since water molecules on hydrophobic surfaces of the free domains are released when the complex forms, the entropy change upon complex formation is usually positive (*16*, *17*). For the ACTR/CBP complex, the negative entropy change is probably due to the loss of conformational freedom and compaction of the peptide backbone upon binding and concomitant folding; these negative contributions cannot be overcome by the favorable entropic contribution of the solvent. The mutation of Arg2105 to Leu in CBP results in a more favorable entropy change upon complex formation (*15*), which can be explained by the more compact structure of

† Supported by grant CA96865 from the National Institutes of Health and by the Skaggs Institute for Chemical Biology. M.O.E. was supported by a fellowship from the Swiss National Science Foundation and S.H.B. by the Korea Research Foundation Grant funded by the Korean Government (MOEHRD, Basic Research Promotion Fund) (KRF-2006-352-C00036).

* Corresponding author. Tel 858 784 9721, fax 858 784 9822, e-mail wright@scripps.edu.

‡ Present address: Institute of Organic Chemistry and Center for Molecular Biosciences, Leopold-Franzens University, Innrain 52a, A-6020 Innsbruck, Austria.

[1] Abbreviations: ACTR, activator for thyroid hormone and retinoid receptors; CBP, CREB binding protein; CREB, cAMP response element-binding; SRC, steroid receptor coactivator; NMR, nuclear magnetic resonance; NOE, nuclear Overhauser effect; $R_1(=1/T_1)$, longitudinal relaxation rate; $R_2(=1/T_2)$, transverse relaxation rate.

10.1021/bi701767j CCC: $40.75
Published on Web 01/05/2008

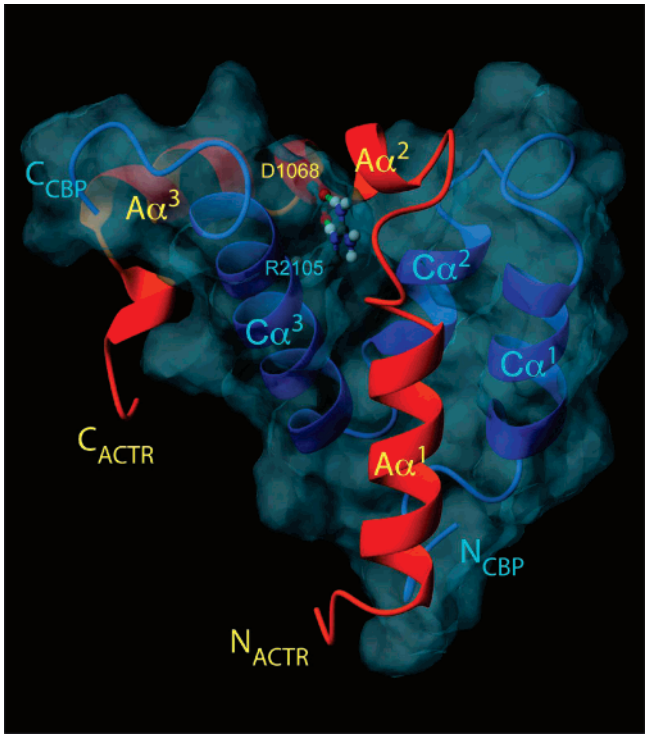

FIGURE 1: Solution structure of the complex between the segment including residues 2059−2117 of CBP (blue) and the activation domain, residues 1041−1088 of the nuclear hormone receptor coactivator ACTR (red) (*14*) (pdb accession code 1kbh). R2105 of CBP and D1068 of ACTR form a buried salt bridge.

the free mutant CBP domain. An additional mutation, Asp1068 of ACTR to Leu, even leads to a slightly positive entropy change upon complex formation, presumably because of more favorable desolvation (*15*). The K_d for complex formation of these two mutant proteins (20 nM) is comparable to the wild type value, illustrating that the thermodynamics of complex formation are affected by the free domain structures.

Simple calorimetric measurements alone cannot provide us with information about the relative entropic contributions of solvent effects and the loss of conformational freedom to the free energy of folding. NMR relaxation measurements (*18*−*20*) allow us to directly probe the dynamics of proteins in their free and bound forms and draw conclusions about the redistribution of conformational entropy upon folding (*21*, *22*). For the ACTR/CBP complex, it is especially interesting to know whether the dynamic behavior is the same as that of an ordinary globular protein complex or if aspects of the dynamic behavior of the free domain are retained in the complex in order to compensate for the entropy loss. Since the free ACTR and CBP domains differ in their secondary structural contents (*14*), we also attempted to correlate this difference with a difference in internal motion. Further, since denaturants influence the conformational ensemble of unfolded states, this complex provided us with an excellent opportunity to study the dynamics of folded and unfolded protein domains under the same, nondenaturing conditions.

MATERIALS AND METHODS

Protein Expression and Sample Preparation. The ACTR domain from human p160 (hACTR(1018−1088) or hACTR-(1041−1088)) and the nuclear coactivator domain of mouse CREB-binding protein (mCBP(2059−2117)) were coexpressed in *E. coli* as described previously (*14*). The harvested cells were lysed by sonication, and the proteins were purified separately using reverse phase HPLC. The lyophilized proteins were dissolved in 0.5 mL of phosphate buffer (50 mM, pH 8.0, 50 mM NaCl) and dialyzed against the NMR buffer (10 mM phosphate pH 6.7, 50 mM NaCl). For relaxation experiments on the complex, ^{15}N-labeled and unlabeled binding partners were mixed in 1:2 molar ratio. Unless otherwise indicated, the concentration of the labeled domain was 0.5 mM. Experiments using hACTR(1018−1088) were performed in Tris buffer (pH 6.7, 50 mM NaCl). Double-labeled protein samples were prepared for the backbone assignment of the free domains (1 mM protein concentration, 10 mM phosphate or Tris buffer pH 6.7, 50 mM NaCl). Diffusion experiments were performed in D_2O with a small amount of dioxane added as internal reference. All other spectra were recorded in 90% H_2O/D_2O.

NMR Spectroscopy. NMR experiments were performed on Bruker DRX 500 and 600 spectrometers equipped with 5 mm triple-resonance cryogenic probe heads with *z*-gradients, and on a Bruker DRX 750 spectrometer equipped with a regular 5 mm triple-resonance probe head with *z*-gradients. The sample temperature was 31 °C.

Resonance Assignments. Backbone resonance assignment was accomplished by using HNCACB, CBCA(CO)NH, (HCA)CO(CA)NH, and HNCO experiments for hACTR-(1018−1088), and HNCA, HN(CO)CA, HNCACB, (HCA)-CO(CA)NH, and HNCO experiments for mCBP(2059−2117) (*23*, *24*). Transfer of the assignments to hACTR(1041−1088) was confirmed using ^{1}H-^{15}N−TOCSY-HSQC and ^{1}H-^{15}N-NOESY-HSQC.

T_1, T_2, and [^{1}H]−^{15}N NOE Measurements. Published pulse sequences for T_1, T_2, and [^{1}H]−^{15}N steady-state nuclear Overhauser effect (NOE) experiments were used (*25*, *26*). Saturated and unsaturated spectra for the determination of the [^{1}H]−^{15}N NOE were recorded in an interleaved manner. The spectral width in the direct dimension was 16 ppm. The indirect dimension was centered around 117 ppm with a spectral width of about 22 ppm. For the complex containing hACTR(1018−1088), 2048 complex data points with 128 complex increments were collected. For all relaxation experiments using the hACTR(1041−1088), spectra with 64 complex increments were recorded. Typically, 8 scans per increment were collected for T_1 and T_2 experiments and 16 scans for [^{1}H]−^{15}N NOE experiments. The minimal recycle delay was 3.5 s. For saturation of the ^{1}H nuclei in the [^{1}H]−^{15}N NOE experiments, 120° pulses separated by 18 ms were applied for 3 s. In order to estimate the error in the [^{1}H]−^{15}N NOE, a minimum of three sets of spectra were recorded. The 180° pulses in the CPMG pulse train of the T_2 experiment were separated by 1 ms. For most T_1 experiments, the relaxation delays were set to 10*, 150, 300*, 450, 600*, 750, and 1000 ms. For typical T_2 experiments, the delays were set to 4, 40*, 80*, 120, 160*, and 200 ms (the asterisks denote duplicate measurements). A minimum of seven time points and three duplicates were used for the determination of all T_1 relaxation times and at least six time points and three duplicates were measured to determine the T_2 relaxation rates. Spectra were processed using nmrPipe2.1 (*27*). The number of complex increments in the indirect dimension was doubled by linear prediction. Zero filling to twice the data

size was applied in both dimensions. The spectra were apodized using a shifted sine-bell function. Cross-peak intensities were measured as the average of the peak maximum and the two adjacent points in each dimension. This was done with the program peakfit (Jonathan C. Lansing, unpublished) using the nmrPipe spectrum files. An exponential function of the form $I_t = I_0 \exp(-tR_n)$, where R_n is the R_1 or R_2 relaxation rate, was fitted to the decay curves of the T_1 and T_2 peak intensities using the program CURVEFIT (A. Palmer, Columbia University). A uniform error for the intensity of a cross-peak was estimated by calculating the square root of the average of the squared uncertainties (standard deviation or difference) of the repeated time points. The $[^1H]-^{15}N$ NOE was calculated from the ratio of the peak intensities in the saturated and unsaturated spectra. The standard deviation for every cross-peak was calculated directly from the repeated measurements.

Transverse Cross-Correlation. Published pulse sequences were used for the determination of transverse cross-relaxation rates (*28*). The spectral width in the direct dimension was 16 ppm. The indirect dimension was centered at 117.5 ppm with a spectral width of 22 ppm for the sample containing ^{15}N-labeled ACTR and 19 ppm for the sample containing ^{15}N-labeled CBP. The data matrix consisted of 32 (t_1) and 2048 (t_2) complex points. For experiment B (reference spectrum) 64 scans per complex increment were collected, while 256 scans were acquired for experiment A (*28*). Durations of the dephasing delay 2Δ were 32*, 53.4, 74.8, and 96.1* ms (time points denoted with an asterisk were measured three times). The recycle delay was set to 1.2 s. The cross-correlation rate was calculated by fitting the function $\tanh(2\Delta\eta)$ to the ratio I_A/I_B of the peak intensities in the cross-correlation spectra A and B. This ratio was corrected for the different number of scans in the two experiments. A uniform variance for the intensities of a cross-peak in one kind of spectrum was estimated by taking the average of the variances of the repeated time points. The fitting was done using the program CURVEFIT.

Translational Diffusion and Hydrodynamic Radius. Relative diffusion coefficients were measured using the PG-SLED (pulse gradient stimulated echo longitudinal encode-decode) sequence (*29*). A series of 18 1D spectra with varying strength of the diffusion gradients (5−100%) was recorded as a pseudo 2D spectrum (for the free CBP domain each of the 1D spectra was repeated three times). The spectral width was 16 ppm, and 128 scans were acquired per spectrum. The diffusion delay was set to 58 ms. The length of the diffusion gradients was 6.5 ms. The length of the crush gradient pulses was 1 ms at a strength of 50%. The relative diffusion coefficient, d, was obtained by fitting the function $A\exp(-dG^2)$ to the signal intensity $I(G)$ in the aromatic region of the PG-SLED spectrum (G being the relative gradient strength). Using the dioxane signal, a reference value d_{ref} was calculated. Assuming that the hydrodynamic radius $R_{H(ref)}$ of the reference molecule is known and not strongly dependent on solution conditions and temperature, we can calculate R_H of the protein using the formula: $R_H = (R_{H(ref)})-(d_{ref}/d)$. The hydrodynamic radius of dioxane was assumed to be 2.12 Å (*30*) and temperature independent in the range between 20 and 31 °C.

Reduced Spectral Density Functions and Model-Free Analysis. Reduced spectral density mapping was carried out using an in-house program assuming that $J(\omega)$ is proportional to $1/\omega^2$ at high frequency around ω_H. Chemical exchange effects on T_2 relaxation will contribute to $J(0)_{eff}$ (*31, 32*). For model-free analysis, R_1, R_2, and $[^1H]-^{15}N$ NOE data collected at both 500 and 600 MHz were analyzed by the extended Lipari−Szabo formalism (*33*) using an in-house program which implements five models (model 1: S^2; model 2: S^2,τ_e; model 3: S^2,R_{ex}; model 4: S^2,τ_e,R_{ex}; model 5: S^2_f,S^2_s,τ_e) and model selection using a Bayesian information criterion (*34, 35*) after excluding unrealistic models (i.e., any model containing $S^2>1$ or $\tau_e > 50$ ns, or $R_{ex} < 0$) (*36*) (Bae, S. H., manuscript in preparation). Minimum relative errors for R_1 and R_2 were set to 5% of the measured rates and the minimum absolute error for $[^1H]-^{15}N$ NOE was set to 0.05. Chemical shift anisotropy and amide NH bond length were assumed to be −170 ppm and 1.02 Å respectively for all residues. Internal motional parameters (S^2_f, S^2_s, τ_e, R_{ex}) and axially symmetric rotational diffusion tensor parameters (D_{zz}, $D_{xx}(=D_{yy})$, ϕ, θ) were optimized iteratively. Only residues within α helices (1044−1055, 1064−1070, 1073−1079 in ACTR; 2067−2076, 2086−2091, 2095−2110 in CBP) were used for optimizing the rotational diffusion tensor. Since the relaxation data sets of ACTR and CBP were obtained from two protein complexes with different combinations of ^{15}N labeling, the model-free analysis was performed separately for each data set.

RESULTS AND DISCUSSION

Resonance Assignment of the Free ACTR and CBP Domains. Poor chemical shift dispersion causes difficulty in the sequence-specific resonance assignment for unstructured proteins (*37*). For the resonances of completely unfolded proteins, this disadvantage is alleviated by narrower line widths, due to longer T_2 relaxation times, and since individual ^{15}N and ^{13}CO chemical shifts in the unfolded state are influenced both by residue type and local sequence (*38*), these nuclei can be used as a basis for backbone assignments in unfolded proteins. For free hACTR(1018−1088) and mCBP(2059−2117), information from HNCACB and CBCANH spectra was augmented with ^{13}CO correlations from (HCA)CO(CA)NH and HNCO experiments, allowing assignment of most of the backbone $^1H(N)$, ^{15}N, and ^{13}CO resonances as well as the Cα and Cβ resonances (BMRB entries: 15397 and 15398 for the free hACTR(1018−1088) and the free mCBP(2059−2117), respectively. Cβ resonances only for free ACTR). Resonance assignments of the free hACTR(1041−1088) were transferred from hACTR(1018−1088). Assignments for the complex of hACTR(1041−1088) and mCBP(2059−2117) have been reported previously (*39*) (BMRB entry: 5228).

Secondary Chemical Shifts of Free and Complex Forms. Circular dichroism (CD) data of the two free domains (hACTR(1018−1088) and mCBP(2059−2117)) showed that unbound CBP contains more residual helical structure than unbound ACTR (*14*). In agreement with this finding, the Cα and CO secondary chemical shifts show that unbound ACTR is devoid of any secondary structure whereas the first two helices observed in the ACTR complex of CBP (Cα1 and Cα2) are fully formed in the free protein (Figure 2); indeed, Cα2 in the free CBP domain even appears to be extended at its N-terminus to incorporate the glutamine-rich region into the helical structure. The N-terminal half of Cα3 in the free

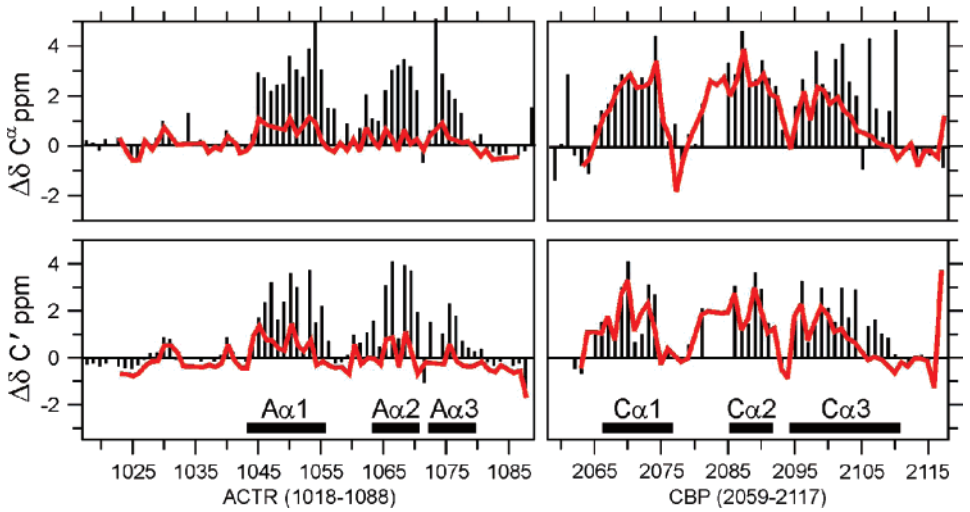

FIGURE 2: Cα and CO secondary chemical shifts of bound (black bars) and free (red lines) forms of hACTR(1018−1088) and mCBP-(2059−2117). The shifts are sequence-corrected (*56*), using random coil shifts (*57*, *58*). The horizontal bars indicate the location of helices Aα1−3 of ACTR and Cα1−3 of CBP in the complex.

protein shows high levels of α-helical content, but it becomes increasingly unstructured toward the C-terminus. This lack of secondary structure at the C-terminal part of Cα3 in the free form is partly explained by the positive charge of the R2105 which appears to inhibit favorable packing of Cα3 against the other two helices of the free CBP domain. Calorimetric studies showed that a mutation R2105L of CBP leads to a stabilization of the free domain and an increase in helix content as measured by CD (*15*). In the complex, Cα3 of the CBP domain is stabilized by interaction with three α-helices of the ACTR domain (Aα1, Aα2, and Aα3). In particular, R2105 of CBP and D1068 of ACTR form a buried salt bridge, and K2108 forms intermolecular hydrogen bonds with T1059 of ACTR, contributing to the specificity of binding (*14*).

The binding interface between hACTR(1018−1086) and mCBP(2059−2117) is mostly hydrophobic and covers about 1500 Å^2 (*14*). The enthalpy change (ΔH) upon complex formation is estimated as −31.5 kcal/mol based on the correlation between buried nonpolar surface area (ΔA) and decrease in binding free energy (correlation coefficient = 21 cal/mol/A^2) (*40*). This estimated ΔH is very close to the experimental ΔH (−31.7 ± 1.5 kcal/mol), indicating that most of the enthalpy change comes from formation of the binding interface. Similarly, the entropy change (ΔS) is estimated by the hydrophobic effect (HE, $0.32\Delta A \ln(T/386) = +114.6$ cal/mol/K), rotation-translation (rt, −50 cal/mol/K), and other effects (e.g., change of conformational flexibility) (*41*). Since the experimentally determined ΔS is −70 cal/mol/K ($T\Delta S = -21.3 \pm 1.5$ kcal/mol, $T = 304$ K) (*14*), the contribution from conformational flexibility will be −134.6 cal/mol/K (ΔS(conformation) = $\Delta S - \Delta S$(HE) − ΔS(rt)). Since the average entropy cost per residue for a folding transition is ∼5.6 cal/mol/K (*41*), the estimated ΔS arising from changes in conformational flexibility corresponds to the entropic cost of folding 24 residues. The changes in secondary chemical shifts between free and bound hACTR(1018−1088) (Figure 2) show that approximately 26 residues fold into helical structure upon binding to the CBP domain. These thermodynamic considerations suggest that the dominant contribution to ΔS upon complex formation is from folding of the unstructured hACTR activation domain. The CBP domain retains a considerable amount of residual secondary structure even in the free form; folding transitions are largely restricted to a small number of residues near the C-terminus of helix Cα3 and appear to contribute relatively little to the overall entropic cost of complex formation.

All of the available data on mCBP(2059−2117) indicates that, while helical structure is present, there is no cooperatively folded structure in the free state. Nevertheless, an NMR structure of a similar CBP construct (mCBP(2067−2112)) in its free form has been reported (*42*). The helical regions of this free CBP structure match well with the helical regions inferred in this work from the secondary chemical shifts of the free protein, but the calculated structure shows a very different topology from that of mCBP(2067−2112) in the ACTR complex (*14*) or the analogous complex with SRC-1 (*43*). This discrepancy probably reflects the high degree of disorder and conformational averaging in the free CBP domain.

NMR Relaxation of the Free Domains. The secondary chemical shifts (Figure 2) and R_1 and R_2 relaxation rates and [^{1}H]−^{15}N NOEs of the hACTR(1018−1088) in the complex (data not shown) suggest that more than 20 residues at the N-terminus are unstructured. Because of known difficulties in the treatment of relaxation data from proteins with long unstructured regions (*44*), the N-terminal 23 residues of the hACTR(1018−1088) were truncated to make a shorter construct, hACTR(1041−1088) for further analysis; the mCBP(2059−2117) domain was left unchanged.

The limited chemical shift dispersion and the lack of cooperative unfolding upon temperature or urea denaturation suggest that both ACTR and CBP domains are disordered in their free states. In fact, R_1 and R_2 relaxation rates and [^{1}H]−^{15}N NOEs strongly support this notion (Figure 3). For the free ACTR domain, all [^{1}H]−^{15}N NOE values are negative and all R_2 values lie in a narrow range below 5 s^{-1}. Interestingly, the [^{1}H]−^{15}N NOE values show a marked dip for residues belonging to the loop region between helices Aα1 and Aα2 of the bound state, even though R_2 and [^{1}H]−^{15}N NOE as well as secondary chemical shifts show that the free ACTR domain is overall fully unfolded.

For the free CBP domain, the differences in the relaxation rates between the free and bound states are much smaller

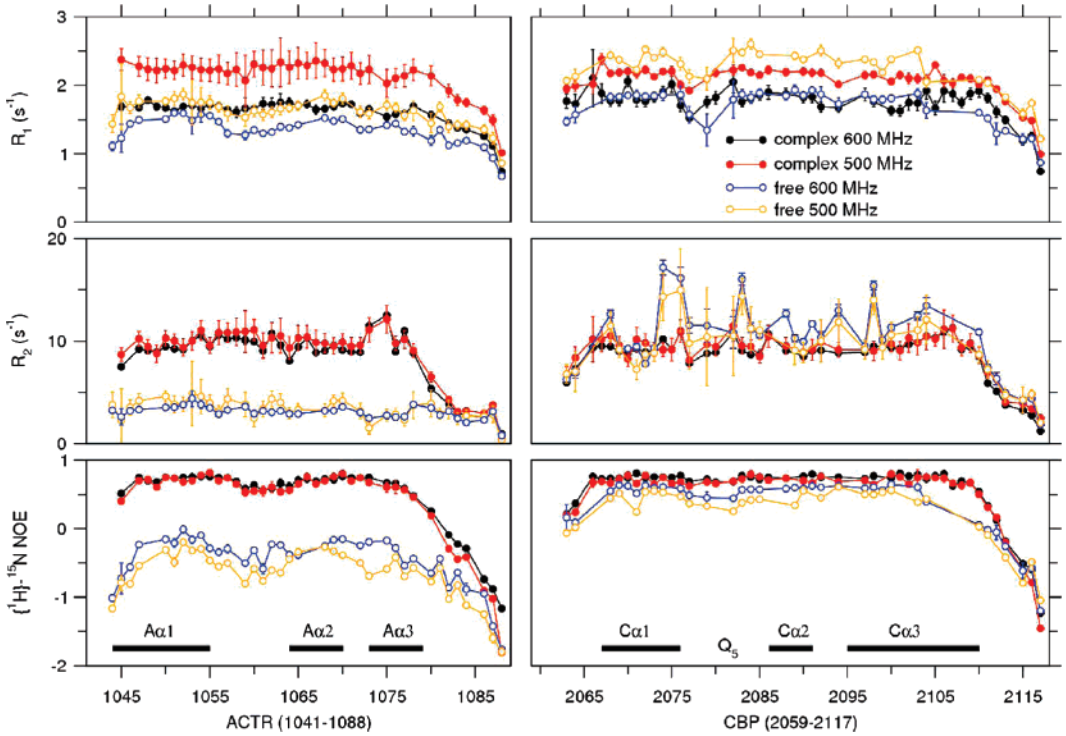

FIGURE 3: ^{15}N R_1, R_2, [^{1}H]−^{15}N NOE of the backbone amides of hACTR(1041−1088) and mCBP(2059−2117) in their free and complex forms. The horizontal bars indicate the helices Aα1−3 of ACTR and Cα1−3 of CBP in the complex. For the free forms, relaxation data were collected at 500 (yellow) and 600 (blue) MHz with ^{15}N-labeled proteins (0.5 mM for ACTR and 1.0 mM for CBP domains) in 10 mM phosphate buffer pH 6.7, 50 mM NaCl at 31 °C. For the complex, relaxation data were collected at 500 (red) and 600 (black) MHz with ^{15}N-labeled proteins (0.5 mM) and unlabeled binding partner (1.0 mM) in 10 mM phosphate buffer (pH 6.7) and 50 mM NaCl at 31 °C.

than those of the ACTR domain. This is consistent with the CBP domain forming a compact molten globule state in its free form (*14*, *15*). We performed pulsed field gradient diffusion experiments to rule out the possibility that dimerization might contribute to the relaxation properties of the free CBP domain. An effective hydrodynamic radius R_H of 17.4 Å was obtained for a 1 mM solution at 31 °C. Using empirical relationships between R_H and the number of amino acids (*30*), we expect R_H to be 15.5 Å for a fully globular CBP monomer and 18.5 Å for a homodimer. Since CBP is a molten globule, the actual R_H will be slightly larger than 15.5 Å, in accord with experimental observation. Indeed, the radius of molten globule states is typically increased by 10−20% relative to the native state (*45*, *46*), so that the expected R_H of the free molten globular CBP domain is between 17 and 19 Å for a monomer and 21−23 Å for a dimer. We thus conclude that the free CBP behaves as a monomer under the conditions of our experiments.

The [^{1}H]−^{15}N NOEs of the free CBP domain at both 500 and 600 MHz are uniformly smaller than those of the bound form, indicative of significant backbone motion in the free form; these motions become restricted upon formation of the complex with CBP. However, about 10 residues at the C-terminus of the Cα3 helix show a significant increase in the [^{1}H]−^{15}N NOE in the complex compared to the free form, which is consistent with the secondary chemical shift data which show an increase in helical structure in Cα3 upon complex formation. In contrast to the free ACTR domain, the R_2 rates are almost identical for most residues in the free and bound states within experimental uncertainties. However, several residues in the C-terminus of Cα1 (T2074, K2076), in the linker between Cα1 and Cα2 (Q2083), and in the N-terminus of Cα3 (M2098) have significantly larger R_2 relaxation rates in the free protein compared to the bound form. Enhanced R_2 relaxation in these regions is likely due to μs−ms time scale fluctuations in the uncomplexed CBP domain, consistent with its molten globule character.

The internal mobility of the free ACTR and CBP domains was characterized with reduced spectral density functions of the NH vectors (*26*, *31*, *32*, *47*, *48*) (Figure 4). $J(0)_{eff}$, which is an indicator for both fast sub-nanosecond motions and exchange processes on the μs−ms time scale, is uniformly low (<1 ns/rad) in free ACTR and clearly differs greatly from that of the bound form. In addition, the free ACTR domain showed high $J(0.87\omega_H)$ values, which together with the low $J(0)_{eff}$ values, indicate significant internal mobility and very fast local tumbling of the free ACTR, supporting the absence of fixed structure in the free form. In the complex, however, the ACTR and CBP domains have almost identical $J(0)_{eff}$ values, which confirms the formation of a globular structure in which backbone motions are highly restricted. In contrast to the ACTR domain, the differences in $J(0)_{eff}$ between the free and bound CBP forms are small implying that overall molecular tumbling of the free and bound forms are similar. However, as observed from R_2 relaxation rates, several residues (T2074, K2076, Q2083, and M2098) in the free CBP domain have significantly elevated $J(0)_{eff}$ values, indicative of μs−ms chemical exchange processes in the uncomplexed state.

NMR Relaxation in the Complex. The ^{15}N-relaxation data for the backbone amides in the complex are also shown in Figure 3. To ensure the complete binding of the ^{15}N-labeled hACTR(1041−1088) or ^{15}N-labeled mCBP(2059−2117) to the unlabeled binding partner, a 2-fold excess of unlabeled protein was added to the ^{15}N-labeled protein for the relaxation measurements. The [^{1}H]−^{15}N NOE provides information

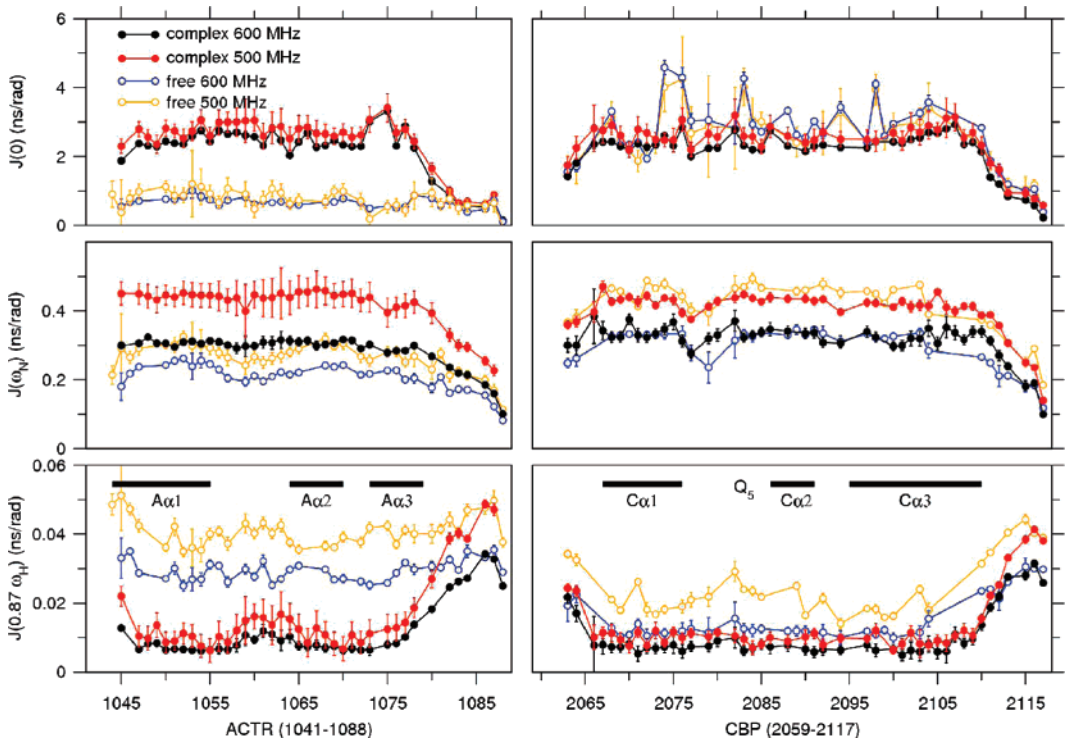

FIGURE 4: Reduced spectral densities calculated from the ^{15}N backbone relaxation data of hACTR(1041−1088) and mCBP(2059−2117) in the free and complex forms. 500 and 600 MHz data were shown in yellow and blue for the free forms and red and black for the complex, respectively. The horizontal bars indicate the helices Aα1−3 of ACTR and Cα1−3 of CBP in the complex.

about the mobility of the backbone NH bond on a ps−ns time scale, decreasing with increasing flexibility of the backbone. The residues in the turn between helices Aα1 and Aα2 showed a slight but significant [^{1}H]−^{15}N NOE decrease, indicating increased mobility of this region in the complex. R_2 shows sequence dependent variations that parallel the [^{1}H]−^{15}N NOE, with small R_2 values in the flexible tails. R_1 exhibits less pronounced changes along the sequence. The [^{1}H]−^{15}N NOEs and relaxation rates for the amide groups of the CBP domain show little variation over the entire domain except for the C-terminal residues following helix Cα3, which are unstructured in the complex.

The spectral densities for the complex were calculated using reduced spectral density mapping (*26*, *31*, *32*, *47*, *48*) (Figure 4). $J(0)_{\text{eff}}$ and $J(0.87\omega_H)$ are important indicators for the presence of exchange processes and motion in the subnanosecond regime (*49*). For a completely rigid molecule, $J(0)_{\text{eff}} = J(0)$ is $^2/_5\tau_c$. Exchange processes on the time-scale of μs to ms increase $J(0)_{\text{eff}}$ whereas fast internal motions in the picosecond regime have the opposite effect. $J(0.87\omega_H)$ is derived directly from R_1 and the [^{1}H]−^{15}N heteronuclear NOE without making use of R_2 relaxation rates and is therefore unaffected by exchange processes. Fast motions on the picosecond time scale result in an increase of $J(0.87\omega_H)$.

The small $J(0)_{\text{eff}}$ values for the terminal residues of the ACTR and CBP domains point to a larger flexibility of these regions, which is also consistent with the [^{1}H]−^{15}N NOE data and increased $J(0.87\omega_H)$ values. Besides the terminal regions, higher values for $J(0.87\omega_H)$ are observed at the turn between Aα1 and Aα2, implying significant internal motions in this region. The structured parts of the CBP domain exhibit only minor fluctuations in $J(0.87\omega_H)$.

Overall Molecular Tumbling of the Complex. Lipari and Szabo introduced a parametrization of the spectral density function based on the assumption that the correlation function of a bond vector can be described as the product of two independent correlation functions for molecular tumbling and internal motion (*50*). The internal correlation function is then represented as a function of so-called 'model-free' parameters which describe internal dynamics in a general, model-independent way (*33*, *50*). The use of this model-free formalism for the analysis of relaxation data allows the determination of amplitudes and correlation times of local motions.

A good initial estimate of the molecular tumbling time or rotational correlation time τ_c of the molecule is important for accurate analysis using the model-free approach. In most cases it is possible to obtain a fairly accurate estimate of τ_c from R_2/R_1 ratios of residues which neither take part in extended sub-nanosecond motion nor undergo μs−ms chemical exchange processes. According to the model-free theory, the local correlation time $\tau_{c,i}$ can then be described (*51*) as:

$$\tau_{c,i} = (2\omega_N)^{-1}(6(R_2/R_1)_i - 7)^{1/2}$$

The rotational correlation time calculated from the trimmed average of the R_2/R_1 ratio is 6.8 ns for the complex. In order to rule out the formation of concentration-dependent aggregates, we determined the trimmed average of R_2 of the hACTR(1041−1088) in the complex at different total protein concentrations and molar ratios (Table 1). The average R_2 values were essentially unchanged over the range of conditions tested except for the complex with a total protein concentration of 3 mM, for which the higher viscosity of the protein solution is likely to affect molecular tumbling significantly.

Table 1: Average R_2 of the ^{15}N-Labeled hACTR(1041−1088) in the Complex with Unlabeled mCBP(2059−2117) in Different Molar Ratios and Concentrations

ACTR (mM)	CBP (mM)	total protein (mM)	molar ratio (ACTR:CBP)	average R_2 (s^{-1})
0.35	0.42	0.77	1:1.2	9.7 ± 1.9
0.5	1.0	1.5	1:2	9.6 ± 0.8
0.25	1.25	1.5	1:6	9.7 ± 1.1
0.5	2.5	3.0	1.5	11.1 ± 1.1

For an independent estimate of τ_c, we determined the effective hydrodynamic radius (R_H) of the 1:1 complex of hACTR(1041−1088)/mCBP(2059−2117) in a 1 mM sample by using the Stokes−Einstein equation and pulse field gradient translational diffusion measurements (*29*). R_H is defined as the radius of a sphere with the same translational self-diffusion constant as the molecule under investigation. The R_H of the ACTR/CBP complex was determined to be 18.1 ± 0.1 Å, based on the R_H of dioxane (2.12 Å) which was used as an internal reference (*30*). Assuming that the ACTR/CBP complex is spherical in shape, and that the viscosity of the protein solution is the same as for pure H_2O at 31 °C (0.008 poise) (*Handbook of Chemistry and Physics*, 63rd ed.), a rotational correlation time τ_c of 4.7 ± 0.8 ns (at 304 K) can be derived using: $\tau_c = 4\pi\eta R_H^3/(3kT)$ in which T is the temperature in Kelvin, k is the Boltzmann constant, and η is the viscosity of the solution.

We attempted to reproduce this R_H value by hydrodynamic simulation using HYDRONMR (*52*) and the atomic coordinates of the hACTR(1040−1086)/mCBP(2059−2117) complex (pdb id: 1kbh) (*14*). The experimental R_H that is derived from the translational diffusion measurement was reproduced when the atomic element radius (AER) in the simulation was set to 2.5 Å if the solution viscosity is 0.008 poise at 304 K. It has been argued that deviations from the consensus AER value of 3.3 Å should be considered as an indicator for the deviation of the assumed molecular structure from the true structure in solution (*53*). For example, for a protein sample with partial aggregation, the AER needs to be much larger than 3.3 Å, and for molecules containing flexible regions the AER needs to be substantially smaller than 3.3 Å in order to reproduce the experimental data. By removing all the terminal residues from the coordinate file that have negative [^{1}H]−^{15}N NOE, we could exactly reproduce the measured R_H with the consensus AER of 3.3 Å.

The rotational correlation time derived from the translational diffusion coefficient is about 2 ns shorter than that derived from R_2/R_1 ratio. Derivation of the rotational correlation time from the translational diffusion coefficient is based on the assumption that ratio of translational and rotational coefficients is constant. This assumption would be valid for a rigid protein but not for a flexible protein. Relaxation data and spectral density analyses show that about 20% of the residues of the hACTR(1041−1088)/mCBP(2059−2117) complex are highly flexible. Thus, the translational diffusion measurements imply that the hACTR(1041−1088)/mCBP(2059−2117) complex has significant flexibility such that translational and rotational diffusion coefficients are not linearly correlated.

In order to ensure that the discrepancy in the rotational correlation time derived from the R_2/R_1 ratio and from the diffusion coefficient is not caused by a uniform increase in R_2, which might be attributed by pervasive chemical exchange contributions, we determined the transverse cross-correlation rate η_{xy} between ^{1}H−^{15}N dipole−dipole interaction and ^{15}N chemical shift anisotropy (CSA) from the intensity ratio of cross and auto relaxation experiments (*28*, *54*). R_2^0, the R_2 relaxation rate devoid of chemical exchange contributions, was estimated by (*55*):

$$R_2^0 = -\eta_{xy}\sqrt{3}(4c^2 + 3d^2)/12cdP_2(\cos\beta)$$

in which $c = (\omega_N/\sqrt{3})\Delta\sigma$, $d = [\mu_0 h\gamma_N\gamma_H/(8\pi^2)](1/r^3_{NH})$, $P_2(x) = (3x^2 - 1)/2$ is the second rank Legendre polynomial, h is Planck's constant, μ_0 is the permeability of free space, $\Delta\sigma$ is the ^{15}N CSA, and β is the angle between the ^{15}N−^{1}H vector and the principal axis of the ^{15}N chemical shift tensor.

Comparison of R_2 and R_2^0 showed significant chemical exchanges at the terminal residues and the turn regions between the Aα1 and Aα2 and between Cα1 and Cα2 (Figure 5); however, it ruled out a uniform increase of R_2 by pervasive exchange processes.

Model-Free Analysis of the Complex. The model-free analysis was performed using an axially symmetric diffusion tensor. The parameter D_{ratio} (= D_{par}/D_{perp}) was estimated during the analysis (mean value 1.25). The rotational correlation times τ_c (= 1/6D) of ^{15}N-ACTR/unlabeled CBP and unlabeled ACTR/^{15}N-CBP complexes were estimated as 6.86 and 6.56 ns from the R_2/R_1 ratio and after cycles of model selection and optimization, they converged to 6.97 and 6.73 ns, respectively. Fits for 72 out of 85 residues were acceptable at the 95% confidence level.

Most residues have order parameters (S^2) between 0.8 and 0.9 (Figure 6), which is typical for residues in the structured core of a globular protein. Despite the remarkable dynamic differences between the free domains, the average S^2 of the ACTR and CBP domains in the complex are overall quite similar.

The linker region between Aα1 and Aα2 has slightly lower S^2 and slower internal correlation times (τ_e, ∼0.9 ns). This same region also has small chemical exchange terms (R_{ex}, ∼1 s^{-1}) extending into the C-terminus of the Aα1 helix, which is consistent with the ($R_2 - R_2^0$) values obtained from the cross-correlation rates (Figure 5). Taken together, these data indicate that this region is highly dynamic and could serve as a hinge between Aα1 and Aα2−3. Flexibility in this hinge region might facilitate binding to CBP; helices Aα1 and Aα2 dock on opposite faces of the CBP domain and flexibility in the intervening linker may facilitate the search for optimal intermolecular contacts. In accordance with this notion, this linker region has significantly lower [^{1}H]−^{15}N NOE than nearby residues even in the free state (Figure 3), suggesting that its flexibility arises from the nature of the amino acid sequence (-L_{1056}SNTDATG$_{1063}$-) and might play an important role in the coupled folding and binding process. Residues E1075, and V1077 showed R_{ex} values larger than 1.5 s^{-1}, which is also supported by the increased R_2 and $J(0)_{eff}$ values and by ($R_2 - R_2^0$) relaxation rates (Figures 3, 4, and 5). These exchange terms probably reflect fluctuating contacts between the Aα3 helix and the C-terminal end of Cα3 (Figure 7).

The S^2 values are relatively uniform in the structured regions of the CBP domain (Figure 6), with increased

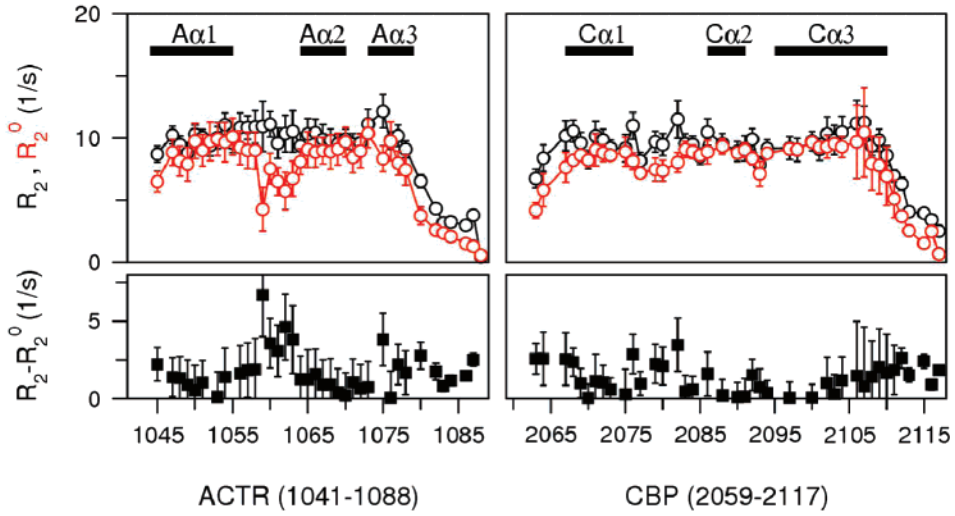

FIGURE 5: R_2 (black) and R_2^0 (red), the R_2 relaxation rate devoid of chemical exchange contributions, of hACTR(1041−1088)/mCBP-(2059−2117) at 500 MHz. For R_2^0 calculations, $\beta = 20°$ and $\Delta\sigma = -170$ ppm and were assumed for all residues (*54*).

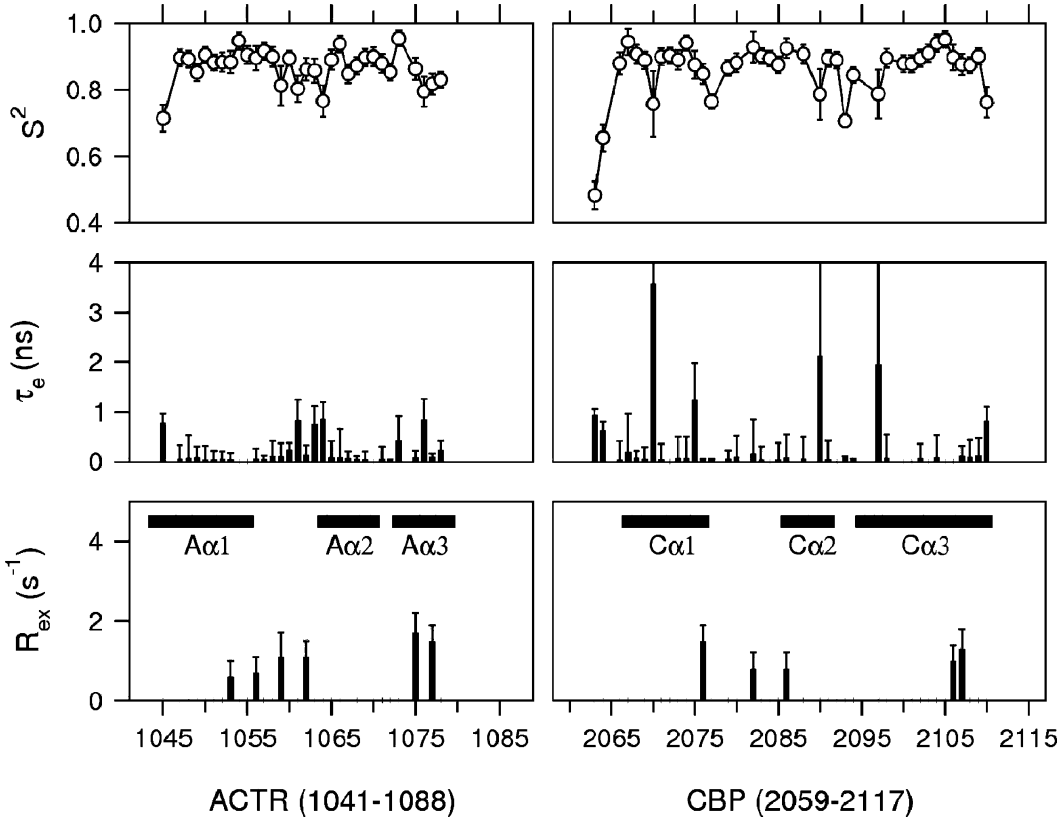

FIGURE 6: Model-free parameters of the hACTR(1041−1088)/mCBP(2059−2117) complex. NMR relaxation data collected at 500 and 600 MHz were analyzed by extended Lipari−Szabo formalism (*33*, *50*). The horizontal bars indicate the helices Aα1−3 of ACTR and Cα1−3 of CBP in the complex.

flexibility evident at the N- and C-termini and, to a more limited extent, in the linkers between Cα1 and Cα2 and between Cα2 and Cα3. Several residues in the Cα1 helix, poly-Q stretch (residues 2082−2086), and Cα2 helix show either slow internal correlation times or R_{ex} around 1 s^{-1}. Overall, however, the dynamics of the CBP is as expected for a globular protein domain.

CONCLUSION

The structure and dynamics of the free and bound forms of the ACTR and CBP domains are distinctively different. The secondary chemical shifts and NMR relaxation data reveal that the free ACTR domain is completely unstructured while the free CBP domain has similar helical secondary structure as in the complex. However, $[^1H]-^{15}N$ NOEs are increased by about 0.2 on average, and chemical exchange processes on the μs−ms time scale are remarkably reduced in the complex compared to the free CBP form, consistent with previous data that show that the free CBP domain is in a molten globule state (*14*). In the complex, α-helical regions of both ACTR and CBP domains show $[^1H]-^{15}N$ NOEs that are typical of folded globular proteins; the spectral densities and R_2^0 also support our conclusion that there is no extensive μs−ms time scale chemical exchange process. Model-free

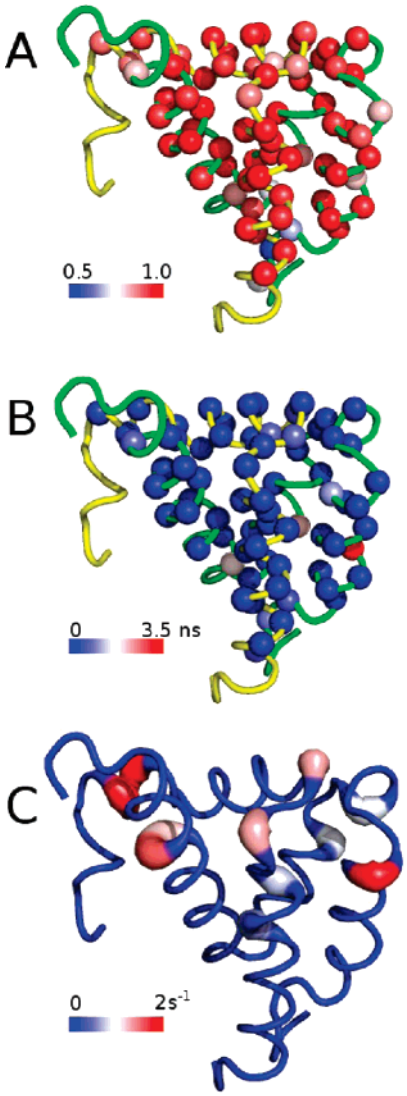

FIGURE 7: Model-free parameters (A) S^2, (B) τ_e, (C) R_{ex} mapped on the hACTR(1041−1088)/mCBP(2059−2117) complex structure. The complex is shown in similar molecular orientation to the Figure 1. In parts A and B, the backbone of mCBP(2059−2117) is shown in green and the backbone of hACTR(1041−1088) in yellow. The range of values for the model-free parameters is depicted by the color spectrum. The radius of the ribbon represents the R_{ex} value in part C.

analysis of the ACTR/CBP complex showed that most residues are highly ordered, except for the linker between Aα1 and Aα2 of ACTR which is flexible in both free and bound forms. By comparing the structure and dynamics between the free and bound forms of ACTR and CBP domains, we have confirmed that ACTR/CBP complex formation involves a synergistic mutual folding process, in which the large conformational entropy cost is not compensated by increased mobility of the backbone in the complex. The partially folded molten globule state of the free CBP appears to be important for controlling the thermodynamics and affinity of complex formation.

ACKNOWLEDGMENT

We thank John Chung, Gerard Kroon, and Markus Zeeb for assistance with NMR experiments and Jianhan Chen for valuable discussions.

REFERENCES

1. Mangelsdorf, D. J., Thummel, C., Beato, M., Herrlich, P., Schütz, G., Umesono, K., Blumberg, B., Kastner, P., Mark, M., Chambon, P., and Evans, R. M. (1995) The nuclear receptor superfamily: the second decade, *Cell 83*, 835−839.
2. Aranda, A., and Pascual, A. (2001) Nuclear hormone receptors and gene expression, *Physiol. Rev. 81*, 1269−1304.
3. Dilworth, F. J., and Chambon, P. (2001) Nuclear receptors coordinate the activities of chromatin remodeling complexes and coactivators to facilitate initiation of transcription, *Oncogene 20*, 3047−3054.
4. Tata, J. R. (2002) Signalling through nuclear receptors, *Nat. Rev. Mol. Cell Biol. 3*, 702−710.
5. Chen, H., Lin, R. J., Schiltz, R. L., Chakravarti, D., Nash, A., Nagy, L., Privalsky, M. L., Nakatani, Y., and Evans, R. M. (1997) Nuclear receptor coactivator ACTR is a novel histone acetyltransferase and forms a multimeric activation complex with P/CAF and CBP/p300, *Cell 90*, 569−580.
6. Leo, C., and Chen, J. D. (2000) The SRC family of nuclear receptor coactivators, *Gene 245*, 1−11.
7. Xu, J., and Li, Q. (2003) Review of the in vivo functions of the p160 steroid receptor coactivator family, *Mol. Endocrinol. 17*, 1681−1692.
8. Anzick, S. L., Kononen, J., Walker, R. L., Azorsa, D. O., Tanner, M. M., Guan, X.-Y., Sauter, G., Kallionemi, O.-P., Trent, J. M., and Meltzer, P. S. (1997) AIB1, a steroid receptor coactivator amplified in breast and ovarian cancer, *Science 277*, 965−968.
9. Xu, J., Liao, L., Ning, G., Yoshida-Komiya, H., Deng, C., and O'Malley, B. W. (2000) The steroid receptor coactivator SRC-3 (p/CIP/RAC3/AIB1/ACTR/TRAM-1) is required for normal growth, puberty, female reproductive function, and mammary gland development, *Proc. Natl. Acad. Sci. U.S.A 97*, 6379−6384.
10. Torres-Arzayus, M. I., Font de, M. J., Yuan, J., Vazquez, F., Bronson, R., Rue, M., Sellers, W. R., and Brown, M. (2004) High tumor incidence and activation of the PI3K/AKT pathway in transgenic mice define AIB1 as an oncogene, *Cancer Cell 6*, 263−274.
11. List, H. J., Lauritsen, K. J., Reiter, R., Powers, C., Wellstein, A., and Riegel, A. T. (2001) Ribozyme targeting demonstrates that the nuclear receptor coactivator AIB1 is a rate-limiting factor for estrogen-dependent growth of human MCF-7 breast cancer cells, *J. Biol. Chem. 276*, 23763−23768.
12. Louie, M. C., Zou, J. X., Rabinovich, A., and Chen, H. W. (2004) ACTR/AIB1 functions as an E2F1 coactivator to promote breast cancer cell proliferation and antiestrogen resistance, *MCB 24*, 5157−5171.
13. Osborne, C. K., Bardou, V., Hopp, T. A., Chamness, G. C., Hilsenbeck, S. G., Fuqua, S. A., Wong, J., Allred, D. C., Clark, G. M., and Schiff, R. (2003) Role of the estrogen receptor coactivator AIB1 (SRC-3) and HER-2/neu in tamoxifen resistance in breast cancer, *J. Natl. Cancer Inst. 95*, 353−361.
14. Demarest, S. J., Martinez-Yamout, M., Chung, J., Chen, H., Xu, W., Dyson, H. J., Evans, R. M., and Wright, P. E. (2002) Mutual synergistic folding in recruitment of CBP/p300 by p160 nuclear receptor coactivators, *Nature 415*, 549−553.
15. Demarest, S. J., Deechongkit, S., Dyson, H. J., Evans, R. M., and Wright, P. E. (2004) Packing, specificity, and mutability at the binding interface between the p160 coactivator and CREB-binding protein, *Protein Sci. 13*, 203−210.
16. Stites, W. E. (1997) Protein-Protein Interactions: Interface Structure, Binding Thermodynamics, and Mutational Analysis, *Chem. Rev. 97*, 1233−1250.
17. Brady, G. P., and Sharp, K. A. (1997) Entropy in protein folding and in protein-protein interactions, *Curr. Opin. Struct. Biol. 7*, 215−221.
18. Ishima, R., and Torchia, D. A. (2000) Protein dynamics from NMR, *Nature Struct. Biol. 7*, 740−743.
19. Korzhnev, D. M., Billeter, M., Arseniev, A. S., and Orekhov, V. Y. (2001) NMR studies of Brownian tumbling and internal motions in proteins, *Prog. Nucl. Magn. Reson. Spectrosc. 38*, 197−266.
20. Palmer, A. G., Kroenke, C. D., and Loria, J. P. (2001) Nuclear magnetic resonance methods for quantifying microsecond-to-millisecond motions in biological macromolecules, *Methods Enzymol. 339*, 204−238.
21. Spyracopoulos, L., and Sykes, B. D. (2001) Thermodynamic insights into proteins from NMR spin relaxation studies, *Curr. Opin. Struct. Biol. 11*, 555−559.

22. Stone, M. J. (2001) NMR relaxation studies of the role of conformational entropy in protein stability and ligand binding, *Acc. Chem. Res. 34*, 379−388.
23. Clore, G. M., and Gronenborn, A. M. (1994) Multidimensional heteronuclear Nuclear Magnetic Resonance of proteins, *Methods Enzymol. 239*, 349−363.
24. Löhr, F., and Rüterjans, H. (1995) A new triple-resonance experiment for the sequential assignment of backbone resonances in proteins, *J. Biomol. NMR 6*, 189−197.
25. Farrow, N. A., Muhandiram, R., Singer, A. U., Pascal, S. M., Kay, C. M., Gish, G., Shoelson, S. E., Pawson, T., Forman-Kay, J. D., and Kay, L. E. (1994) Backbone dynamics of a free and a phosphopeptide-complexed Src homology 2 domain studied by ^{15}N NMR relaxation, *Biochemistry 33*, 5984−6003.
26. Farrow, N. A., Zhang, O., Forman-Kay, J. D., and Kay, L. E. (1995) Comparison of the backbone dynamics of a folded and an unfolded SH3 domain existing in solution in aqueous buffer, *Biochemistry 34*, 868−878.
27. Delaglio, F., Grzesiek, S., Vuister, G. W., Guang, Z., Pfeifer, J., and Bax, A. (1995) NMRPipe: a multidimensional spectral processing system based on UNIX pipes, *J. Biomol. NMR 6*, 277−293.
28. Tjandra, N., Szabo, A., and Bax, A. (1996) Protein backbone dynamics and ^{15}N chemical shift anisotropy from quantitative measurement of relaxation interference effects, *J. Am. Chem. Soc. 118*, 6986−6991.
29. Jones, J. A., Wilkins, D. K., Smith, L. J., and Dobson, C. M. (1997) Characterisation of protein unfolding by NMR diffusion measurements, *J. Biomol. NMR 10*, 199−203.
30. Wilkins, D. K., Grimshaw, S. B., Receveur, V., Dobson, C. M., Jones, J. A., and Smith, L. J. (1999) Hydrodynamic radii of native and denatured proteins measured by pulse field gradient NMR techniques, *Biochemistry 38*, 16424−16431.
31. Farrow, N. A., Zhang, O., Szabo, A., Torchia, D. A., and Kay, L. E. (1995) Spectral density function mapping using ^{15}N relaxation data exclusively, *J. Biomol. NMR 6*, 153−162.
32. Peng, J. W., and Wagner, G. (1995) Frequency spectrum of NH bonds in eglin C from spectral density mapping at multiple fields, *Biochemistry 34*, 16733−16752.
33. Clore, G. M., Szabo, A., Bax, A., Kay, L. E., Driscoll, P. C., and Gronenborn, A. M. (1990) Deviations from the simple two-parameter model-free approach to the interpretation of nitrogen-15 nuclear magnetic relaxation of proteins, *J. Am. Chem. Soc. 112*, 4989−4991.
34. Chen, J., Brooks, C. L., and Wright, P. E. (2004) Model-free analysis of protein dynamics: assessment of accuracy and model selection protocols based on molecular dynamics simulations, *J. Biomol. NMR 29*, 243−257.
35. d'Auvergne, E. J., and Gooley, P. R. (2003) The use of model selection in the model-free analysis of protein dynamics, *J. Biomol. NMR 25*, 25−39.
36. d'Auvergne, E. J., and Gooley, P. R. (2006) Model-free model elimination: a new step in the model-free dynamic analysis of NMR relaxation data, *J. Biomol. NMR 35*, 117−135.
37. Dyson, H. J., and Wright, P. E. (2002) Insights into the structure and dynamics of unfolded proteins from nuclear magnetic resonance, *Adv. Protein Chem. 62*, 311−340.
38. Yao, J., Dyson, H. J., and Wright, P. E. (1997) Chemical shift dispersion and secondary structure prediction in unfolded and partly folded proteins, *FEBS Lett. 419*, 285−289.
39. Demarest, S. J., Chung, J., Dyson, H. J., and Wright, P. E. (2002) Assignment of a 15 kDa protein complex formed between the p160 coactivator ACTR and CREB binding protein, *J. Biomol. NMR 22*, 377−378.
40. Sundberg, E. J., Urrutia, M., Braden, B. C., Isern, J., Tsuchiya, D., Fields, B. A., Malchiodi, E. L., Tormo, J., Schwarz, F. P., and Mariuzza, R. A. (2000) Estimation of the hydrophobic effect in an antigen-antibody protein-protein interface, *Biochemistry 39*, 15375−15387.
41. Spolar, R. S., and Record, M. T. (1994) Coupling of local folding to site-specific binding of proteins to DNA, *Science 263*, 777−784.
42. Lin, C. H., Hare, B. J., Wagner, G., Harrison, S. C., Maniatis, T., and Fraenkel, E. (2001) A small domain of cbp/p300 binds diverse proteins. solution structure and functional studies, *Mol. Cell 8*, 581−590.
43. Waters, L., Yue, B., Veverka, V., Renshaw, P., Bramham, J., Matsuda, S., Frenkiel, T., Kelly, G., Muskett, F., Carr, M., and Heery, D. M. (2006) Structural Diversity in p160/CREB-binding Protein Coactivator Complexes, *J. Biol. Chem. 281*, 14787−14795.
44. Viles, J. H., Donne, D. G., Kroon, G. J. A., Prusiner, S. B., Cohen, F. E., Dyson, H. J., and Wright, P. E. (2001) Local structural plasticity of the prion protein. Analysis of NMR relaxation dynamics, *Biochemistry 40*, 2743−2753.
45. Kataoka, M., Kuwajima, K., Tokunaga, F., and Goto, Y. (1997) Structural characterization of the molten globule of α-lactalbumin by solution X-ray scattering, *Protein Sci. 6*, 422−430.
46. Eliezer, D., Yao, J., Dyson, H. J., and Wright, P. E. (1998) Structural and dynamic characterization of partially folded states of myoglobin and implications for protein folding, *Nat. Struct. Biol. 5*, 148−155.
47. Ishima, R., and Nagayama, K. (1995) Protein backbone dynamics revealed by quasi spectral density function analysis of amide N-15 nuclei, *Biochemistry 34*, 3162−3171.
48. Lefevre, J. F., Dayie, K. T., Peng, J. W., and Wagner, G. (1996) Internal mobility in the partially folded DNA binding and dimerization domains of GAL4: NMR analysis of the N-H spectral density functions, *Biochemistry 35*, 2674−2686.
49. Dayie, K. T., Wagner, G., and Lefèvre, J.-F. (1996) Theory and practice of nuclear spin relaxation in proteins, *Annu. Rev. Phys. Chem. 47*, 243−282.
50. Lipari, G., and Szabo, A. (1982) Model-free approach to the interpretation of nuclear magnetic resonance relaxation in macromolecules. 1. Theory and range of validity, *J. Am. Chem. Soc. 104*, 4546−4559.
51. Fushman, D., Weisemann, R., Thüring, H., and Rüterjans, H. (1994) Backbone dynamics of ribonuclease T1 and its complex with 2′GMP studied by 2-dimensional heteronuclear NMR spectroscopy, *J. Biomol. NMR 4*, 61−78.
52. Garcia de la Torre, J., Huertas, M. L., and Carrasco, B. (2000) HYDRONMR: prediction of NMR relaxation of globular proteins from atomic-level structures and hydrodynamic calculations, *J. Magn Reson. 147*, 138−146.
53. Bernado, P., Garcia, de la Torre, J., and Pons, M. (2002) Interpretation of 15N NMR relaxation data of globular proteins using hydrodynamic calculations with HYDRONMR, *J. Biomol. NMR 23*, 139−150.
54. Fushman, D., Tjandra, N., and Cowburn, D. (1998) Direct measurement of ^{15}N chemical shift anisotropy in solution, *J. Am. Chem. Soc. 120*, 10947−10952.
55. Zeeb, M., Jacob, M. H., Schindler, T., and Balbach, J. (2003) 15N relaxation study of the cold shock protein CspB at various solvent viscosities, *J. Biomol. NMR 27*, 221−234.
56. Schwarzinger, S., Kroon, G. J. A., Foss, T. R., Chung, J., Wright, P. E., and Dyson, H. J. (2001) Sequence dependent correction of random coil NMR chemical shifts, *J. Am. Chem. Soc. 123*, 2970−2978.
57. Wishart, D. S., and Sykes, B. D. (1994) Chemical shifts as a tool for structure determination, *Methods Enzymol. 239*, 363−392.
58. Schwarzinger, S., Kroon, G. J. A., Foss, T. R., Wright, P. E., and Dyson, H. J. (2000) Random coil chemical shifts in acidic 8 M urea: implementation of random coil chemical shift data in NMRView, *J. Biomol. NMR 18*, 43−48.

BI701767J